CHINESE OPTICS LETTERS

Vol. 20, No. 1 | January 2022

Lithium niobate microring with ultra-high Q factor above 10^8

Renhong Gao (高仁宏)[1,6], Ni Yao (姚 妮)[2], Jianglin Guan (管江林)[3,4], Li Deng (邓 莉)[3,4], Jintian Lin (林锦添)[1,6*], Min Wang (汪 旻)[3,4], Lingling Qiao (乔玲玲)[1], Wei Fang (方 伟)[5], and Ya Cheng (程 亚)[1,3,4,6,7,8,9**]

[1] State Key Laboratory of High Field Laser Physics and CAS Center for Excellence in Ultra-Intense Laser Science, Shanghai Institute of Optics and Fine Mechanics, Chinese Academy of Sciences (CAS), Shanghai 201800, China

[2] Research Center for Intelligent Sensing, Zhejiang Lab, Hangzhou 311100, China

[3] XXL—The Extreme Optoelectromechanics Laboratory, School of Physics and Electronic Science, East China Normal University, Shanghai 200241, China

[4] State Key Laboratory of Precision Spectroscopy, East China Normal University, Shanghai 200062, China

[5] State Key Laboratory of Modern Optical Instrumentation, College of Optical Science and Engineering, Zhejiang University, Hangzhou 310027, China

[6] Center of Materials Science and Optoelectronics Engineering, University of Chinese Academy of Sciences, Beijing 100049, China

[7] Collaborative Innovation Center of Extreme Optics, Shanxi University, Taiyuan 030006, China

[8] Collaborative Innovation Center of Light Manipulations and Applications, Shandong Normal University, Jinan 250358, China

[9] Shanghai Research Center for Quantum Sciences, Shanghai 201315, China

*Corresponding author: jintianlin@siom.ac.cn

**Corresponding author: ya.cheng@siom.ac.cn

Received September 9, 2021 | Accepted September 15, 2021 | Posted Online November 3, 2021

We demonstrate integrated lithium niobate (LN) microring resonators with Q factors close to the intrinsic material absorption limit of LN. The microrings are fabricated on pristine LN thin-film wafers thinned from LN bulk via chemo-mechanical etching without ion slicing and ion etching. A record-high Q factor up to 10^8 at the wavelength of 1550 nm is achieved because of the ultra-smooth interface of the microrings and the absence of ion-induced lattice damage, indicating an ultra-low waveguide propagation loss of ~0.0034 dB/cm. The ultra-high Q microrings will pave the way for integrated quantum light source, frequency comb generation, and nonlinear optical processes.

Keywords: lithium niobate; microcavities; waveguide.

DOI: 10.3788/COL202220.011902

1. Introduction

A lithium-niobate-on-insulator (LNOI) wafer is considered as an important candidate platform for photonic integrated circuits (PICs), owing to its outstanding material properties featuring a broad transparency window (350 nm to 5 μm), a linear electro-optic effect, and a large second-order nonlinearity susceptibility ($\chi^{(2)} = 30\,\mathrm{pm/V}$)[1–5]. A wide range of high-performance device applications, such as waveguide/resonator optical frequency convertors, high-speed Mach–Zehnder modulators, and multiplexers, have been demonstrated due to the rapid developments in the ion-slicing technique and LNOI nanofabrication technology[6–23]. Among the various devices, optical waveguides with ultra-low propagation loss and high refractive index contrast are building elements for the realization of large-scale PICs[24–28]. The propagation losses in optical waveguides are susceptible to sidewall roughness induced by the fabrication imperfection. To reduce the sidewall roughness of the waveguide, diamond-blade dicing, precision cutting, focused ion beam milling, argon ion milling, and chemo-mechanical polishing (CMP) have been successively used to etch the lithium niobate (LN) thin film into waveguides with smooth sidewalls to improve propagation losses[29–34]. For instance, an ultra-smooth sidewall roughness as small as 0.1 nm has been achieved by CMP etching, leading to an ultra-low propagation loss of ridge waveguides of 0.027 dB/cm[25,35]. However, the minimum propagation loss of the waveguide determined by the intrinsic material absorption is only 0.001 dB/cm[36]. There is still room to reduce the propagation loss by improving the quality of LN thin film.

In addition to the sidewall-roughness scattering, some other factors, particularly the ion-induced lattice damage caused by ion slicing/milling, should also be taken into account to further reduce the propagation loss[1,4,37]. Particularly, the internal crystal lattice damage induced by the ion-slicing fabrication of the

LN thin film has long been recognized, which represents the ultimate limit of the loss achievable in the traditional ion-sliced LNOI wafer[37,38]. To avoid ion-induced lattice damage, CMP is proposed to produce the LNOI thin-film wafer and ultra-high Q LNOI microdisk. The Q factor as high as 1.23×10^8 at 1550 nm wavelength, which is close to the intrinsic material absorption limit, has been reported[38]. The microring resonators, compared with microdisk resonators, have great advantages due to their superior characteristics such as flexibility in dispersion engineering, capability of electrical integration, and potential for large-scale integration. However, LN, as a difficult-to-cut material, is difficult to be fabricated into a ridge waveguide with low loss.

Here, we challenge the status quo and show that the LN ridge waveguides can be fabricated with a propagation loss as low as 0.0034 ± 0.0001 dB/cm through suppressing the fabrication imperfection during thin-film production and nanostructuring by CMP, which is one order of magnitude lower than the previously reported results[24,25]. The loaded Q factor of the fabricated microring is measured as 0.8×10^8, corresponding to an intrinsic Q factor of 10^8. Remarkably, the microring loss is close to the intrinsic material absorption limit of LN crystals.

2. Fabrication Methods

The manufacturing process for fabricating the LN microrings by CMP is schematically illustrated in Fig. 1, which mainly consists of two consecutive procedures including production of monocrystalline high-quality LN thin-film wafers and nanostructuring of LNOI microrings. To fabricate such LNOI microrings, first, an X-cut LN crystal was bonded to a silica buffer layer at room temperature, where the silica layer with a thickness of 2 μm was deposited on another LN bulk crystal by plasma enhanced chemical vapor deposition. Then, high-temperature annealing at 500°C was performed to enhance the bonding strength. Second, the top bulk crystal was thinned into a 4-μm-thick thin film via CMP, considering the trade-off between the surface evenness and thickness, as shown in Ref. [38]. Thus, combined with the techniques of step 1 and step 2, an LNOI thin-film wafer was formed. Third, to pattern the LN thin film into microrings by CMP etching, a 600-nm-thick chromium (Cr) layer was coated on the LNOI wafer by magnetron sputtering. Fourth, the Cr layer was ablated into a microring-pattern hard mask by femtosecond laser direct writing with a scan speed of 10 cm/s and a pulse width of 190 fs. The laser focal spot was approximately 1 μm, and the thickness of the ablation layer was controlled to be as small as 400 nm by choosing the average power of the laser. Fifth, the sample underwent CMP to etch the exposed LN thin film, leading to the pattern transferring from the Cr layer to LN thin film[39]. Sixth, chemical etching was performed to remove the Cr mask. Finally, a secondary CMP was carried out for thinning the microrings. The main advantage of our fabrication method relies on the optimized process of CMP for thinning LN crystal, alleviating the crystal damage and surface damage.

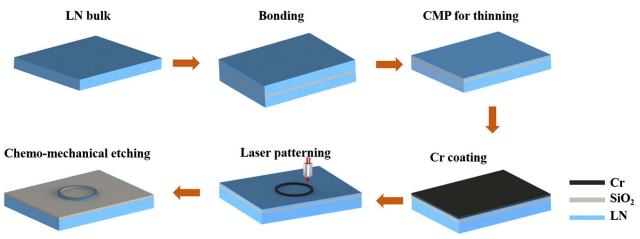

Fig. 1. Illustration of the fabrication flow of the microrings.

3. Characteristics of LN Microrings

The optical microscope image and the magnified scanning-electron-microscope (SEM) image of the microrings are shown in Figs. 2(a) and 2(b), respectively, indicating the LN microring with a diameter of 200 μm and an ultra-smooth surface. To accurately measure the wedge angle and the height of the microrings, a small slit is cut through the microring with a focused ion beam, as shown in Fig. 2(c), showing a wedge angle of 9° and a height of 720 nm. Interestingly, the small wedge angle will drive the modes far from the edge of the microrings, benefiting higher Q factors[40]. As a cost of a small wedge angle, the bottom of the microring is relatively large, which is 20 μm. The waveguide width can be further decreased by choosing thinner film wafers with sub-micron thicknesses[41].

To couple light into and out of the microring, a ridge waveguide with top width, bottom width, and height of 2.11 μm, 9.68 μm, and 700 nm, respectively, is fabricated on a second

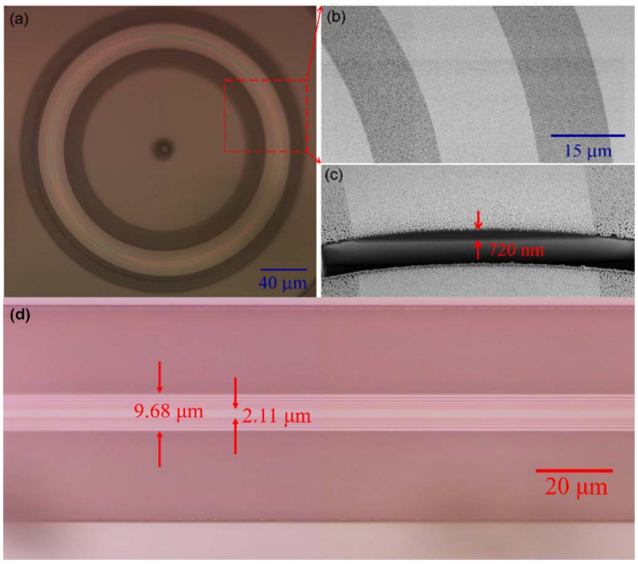

Fig. 2. (a) Optical microscope image of the fabricated microring. (b) Magnified scanning-electron-microscope (SEM) image of the fabricated microring. (c) The SEM image shows that a small slit is cut through the microring with a focused ion beam. (d) The optical microscope image of the ridge waveguide on other LNOI chips for coupling of the microring.

LNOI wafer (produced by ion slicing) by CMP etching, as shown in Fig. 2(d). The experimental setup is schematically illustrated in Fig. 3(a). The ridge waveguide was adjusted to be parallel with the top surface of the microrings by an xyz-θ_x-θ_y rotatability stage and came into contact with the microring to gain optimum coupling, as shown in Fig. 3(b). Lensed fibers were used to couple the light signal into and out of the ridge waveguide by end-fire coupling with a coupling efficiency of 10% per facet. A narrow-linewidth wavelength tunable laser with a linewidth less than 200 kHz (model: TLB-6728, New Focus Inc.) was used as light source with an effective in-coupled power of 5 μW [tuned by a variable optical attenuator (VOA)] in the microring to avoid the thermal and nonlinear optical effects. An inline fiber polarization controller (PC) was used to adjust the polarization of the input light. The output optical signal was coupled out of the microring by the same ridge waveguide and lensed fiber and sent into a photodetector (PD, model: 1811, New Focus Inc.). The transmission spectrum was real-time analyzed by an oscilloscope (model: Tektronix MDO04) when scanning the wavelength of the optical signal. Whispering gallery modes were excited when the optical signal was resonant with the microring, resulting in a spectrum of sharp dips in the transmission spectrum.

Figure 3(c) shows the transmission spectra of the microring at the wavelength ranging from 1566 nm to 1570 nm, exhibiting two sets of high-order transverse electric (TE) and transverse magnetic (TM) modes. The modes were simulated by a finite-element method[42,43] and identified to certain modes according to the free spectral ranges of the modes and the resonant wavelengths of the modes. The refractive indices used in the simulation are calculated using Sellmeier coefficients for congruently grown LN[44]. The two numbers in the subscript of the modes denote the radial (first number) and azimuthal (second number) mode numbers. The free spectral range between modes $TE_{12,736}$ and $TE_{12,737}$ is 1.69 nm, which agrees well with the calculated value of 1.69 nm. The field distributions of the modes $TE_{12,736}$ and $TM_{12,769}$ are plotted in the insets of Figs. 3(d) and 3(e), respectively. The Q factors of the modes $TE_{12,736}$ and $TM_{12,769}$ were characterized using the wavelength tunable laser scanning around the resonant wavelengths, as shown in Figs. 3(d) and 3(e), respectively. The loaded Q factor of the mode $TE_{12,736}$ was measured to be $(4.3 \pm 0.2) \times 10^7$, indicating an intrinsic Q factor of $(5.8 \pm 0.3) \times 10^7$. The mode $TM_{12,769}$ shows a mode splitting with two loaded Q factors of $(5.9 \pm 0.3) \times 10^7$ and $(8.0 \pm 0.3) \times 10^7$ under the condition of near critical coupling, which should be caused by the back reflections inside the ring. Considering the transmission rates of modes, the intrinsic Q factors (Q_i) are $(0.85 \pm 0.04) \times 10^8$ and $(1.08 \pm 0.04) \times 10^8$, respectively, agreeing well with the result of the LNOI microdisks[38]. Remarkably, the highest intrinsic Q factor close to the material intrinsic absorption limit of LN is about one order of magnitude higher than the best-reported values in LNOI microrings[24,25]. The effective index n_{eff} of the mode $TM_{12,769}$ was determined to be 2.10. The corresponding waveguide propagation loss L_P is 0.0034 ± 0.0001 dB/cm, which is calculated by

$$L_p = 10 \cdot \alpha \cdot \log\, e = 10 \cdot (2\pi n_{\text{eff}}/(Q_i \lambda)) \cdot \log e, \tag{1}$$

where α is the material absorption coefficient, and Q_i and λ are the intrinsic Q factor and resonant wavelength of the mode, respectively.

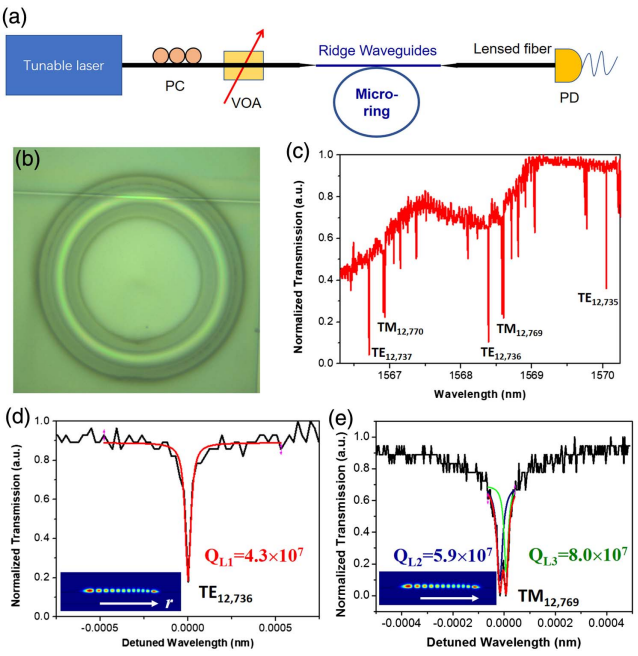

Fig. 3. (a) Experimental setup for mode characterization. (b) Optical micrograph of the waveguide coupled with the microring. (c) The measured transmission spectrum. (d) and (e) Q factors of the modes fitted by Lorentz-shape curves; insets: the corresponding field distributions of the modes, where the direction presents the radial direction.

4. Conclusion

In conclusion, we demonstrate an ultra-high Q microring resonator in LNOI without ion-induced lattice damage by CMP. The intrinsic Q factor above 10^8 was experimentally demonstrated at the 1550 nm wavelength band, while the waveguide propagation loss is only 0.0034 ± 0.0001 dB/cm. This microresonator can be fully integrated with silicon nitride ridge waveguides on chip by vertical coupling[45] or side coupling[46] in the future. This ultra-high Q multimode microring can be used as electro-optic tunable photonic devices, such as low-threshold Kerr frequency combs, narrow-linewidth Brillouin lasers[46], and high-brightness quantum light sources[19], to name a few. Such a low-loss LNOI ridge waveguide shows great potential for lossless cascaded electro-optic modulators, high-speed information processing, and large-scale photonic integration on LNOI wafers.

Acknowledgement

The work was supported by the National Key R&D Program of China (No. 2019YFA0705000), National Natural Science Foundation of China (NSFC) (Nos. 11734009, 11874375, 11874154, and 6212200762), Key Research Program of Frontier Sciences (No. QYZDJ-SSWSLH010), Youth Innovation Promotion Association of Chinese Academy of Sciences (No. 2020249), and Shanghai Municipal Science and Technology Major Project (No. 2019SHZDZX01). We thank the Jingzheng company for producing the thin film by CMP.

References

1. J. Lin, F. Bo, Y. Cheng, and J. Xu, "Advances in on-chip photonic devices based on lithium niobate on insulator," Photon. Res. **8**, 1910 (2020).
2. Y. Qi and Y. Li, "Integrated lithium niobate photonics," Nanophotonics **9**, 1287 (2020).
3. Y. Kong, F. Bo, W. Wang, D. Zheng, H. Liu, G. Zhang, R. Rupp, and J. Xu, "Recent progress in lithium niobate: optical damage, defect simulation, and on-chip devices," Adv. Mater. **32**, 1806452 (2020).
4. Y. Jia, L. Wang, and F. Chen, "Ion-cut lithium niobate on insulator technology: recent advances and perspectives," Appl. Phys. Rev. **8**, 011307 (2021).
5. Y. Zheng and X. Chen, "Nonlinear wave mixing in lithium niobate thin film," Adv. Phys. X **6**, 1889402 (2021).
6. J. Wang, F. Bo, S. Wan, W. Li, F. Gao, J. Li, G. Zhang, and J. Xu, "High-*Q* lithium niobate microdisk resonators on a chip for efficient electro-optic modulation," Opt. Express **23**, 23072 (2015).
7. G. Li, Y. Chen, H. Jiang, and X. Chen, "Broadband sum-frequency generation using d_{33} in periodically poled $LiNbO_3$ thin film in the telecommunications band," Opt. Lett. **42**, 939 (2017).
8. C. Wang, M. Zhang, X. Chen, M. Bertrand, A. Shams-Ansari, S. Chandrasekhar, P. Winzer, and M. Loncar, "Integrated lithium niobate electro-optic modulators operating at CMOS-compatible voltages," Nature **562**, 101 (2018).
9. Y. He, Q.-F. Yang, J. W. Ling, R. Luo, H. X. Liang, M. X. Li, B. Q. Shen, H. M. Wang, K. Vahala, and Q. Lin, "Self-starting bi-chromatic $LiNbO_3$ soliton microcomb," Optica **6**, 1138 (2019).
10. C. Wang, M. Zhang, M. J. Yu, R. R. Zhu, H. Hu, and M. Loncar, "Monolithic lithium niobate photonic circuits for Kerr frequency comb generation and modulation," Nat. Commun. **10**, 978 (2019).
11. B. Mu, X. Wu, Y. Niu, Y. Chen, X. Cai, Y. Gong, Z. Xie, X. Hu, and S. Zhu, "Locally periodically poled LNOI ridge waveguide for second harmonic generation," Chin. Opt. Lett. **19**, 060007 (2021).
12. J. Lin, N. Yao, Z. Hao, J. Zhang, W. Mao, M. Wang, W. Chu, R. Wu, Z. Fang, L. Qiao, W. Fang, F. Bo, and Y. Cheng, "Broadband quasi-phase-matched harmonic generation in an on-chip monocrystalline lithium niobate microdisk resonator," Phys. Rev. Lett. **122**, 173903 (2019).
13. Y. Li, Z. Huang, W. Qiu, J. Dong, H. Guan, and H. Lu, "Recent progress of second harmonic generation based on thin film lithium niobate," Chin. Opt. Lett. **19**, 060012 (2021).
14. A. Rao, K. Abdelsalam, T. Aardema, A. Honardoost, G. F. Camacho-Gonzalez, and S. Fathpour, "Actively-monitored periodic-poling in thin-film lithium niobate photonic waveguides with ultrahigh nonlinear conversion efficiency of 4600 $\%W^{-1}cm^{-2}$," Opt. Express **27**, 25920 (2019).
15. K. Zhang, Z. Chen, H. Feng, W.-H. Wong, E. Y.-B. Pun, and C. Wang, "High-*Q* lithium niobate microring resonators using lift-off metallic masks," Chin. Opt. Lett. **19**, 060010 (2021).
16. J. Lu, J. Surya, X. Liu, Y. Xu, and H. X. Tang, "Octave-spanning supercontinuum generation in nanoscale lithium niobate waveguides," Opt. Lett. **44**, 1492 (2019).
17. Y. Jia, Y. Ren, X. Zhao, and F. Chen, "Surface lattice resonances in dielectric metasurfaces for enhanced light-matter interaction," Chin. Opt. Lett. **19**, 060013 (2021).
18. J. Zhao, C. Ma, M. Ruesing, and S. Y. Mookherjea, "High quality entangled photon pair generation in periodically poled thin-film lithium niobate waveguides," Phys. Rev. Lett. **124**, 163603 (2020).
19. G.-T. Xue, Y.-F. Niu, X. Y. Liu, J.-C. Duan, W. J. Chen, Y. Pan, K. P. Jia, X. H. Wang, H.-Y. Liu, Y. Zhang, P. Xu, G. Zhao, X. L. Cai, Y.-X. Gong, X. P. Hu, Z. D. Xie, and S. N. Zhu, "Ultrabright multiplexed energy-time-entangled photon generation from lithium niobate on insulator chip," Phys. Rev. Appl. **15**, 064059 (2021).
20. B. Fang, S. Gao, Z. Wang, S. Zhu, and T. Li, "Efficient second harmonic generation in silicon covered lithium niobate waveguides," Chin. Opt. Lett. **19**, 060004 (2021).
21. M. Xu, M. He, H. Zhang, J. Jian, Y. Pan, X. Liu, L. Chen, X. Meng, H. Chen, Z. Li, X. Xiao, S. Yu, S. Yu, and X. Cai, "High-performance coherent optical modulators based on thin-film lithium niobate platform," Nat. Commun. **11**, 3911 (2020).
22. Y. F. Niu, C. Lin, X. Y. Liu, Y. Chen, X. P. Hu, Y. Zhang, X. L. Cai, Y.-X. Gong, Z. D. Xie, and S. N. Zhu, "Optimizing the efficiency of a periodically poled LNOI waveguide using *in situ* monitoring of the ferroelectric domains," Appl. Phys. Lett. **116**, 101104 (2020).
23. Z. J. Yu, Y. Y. Tong, H. K. Tsang, and X. K. Sun, "High-dimensional communication on etchless lithium niobate platform with photonic bound states in the continuum," Nat. Commun. **11**, 2602 (2020).
24. M. Zhang, C. Wang, R. Cheng, A. Shams-Ansari, and M. Loncar, "Monolithic ultra-high-*Q* lithium niobate microring resonator," Optica **4**, 1536 (2017).
25. R. B. Wu, M. Wang, J. Xu, J. Qi, W. Chu, Z. W. Fang, J. H. Zhang, J. X. Zhou, L. L. Qiao, Z. F. Chai, J. T. Lin, and Y. Cheng, "Long low-loss-lithium niobate on insulator waveguides with sub-nanometer surface roughness," Nanomaterials **8**, 910 (2018).
26. R. Wolf, I. Breunig, H. Zappe, and K. Buse, "Scattering-loss reduction of ridge waveguides by sidewall polishing," Opt. Express **26**, 19815 (2018).
27. J. T. Lin, J. X. Zhou, R. B. Wu, M. Wang, Z. W. Fang, W. Chu, J. H. Zhang, L. L. Qiao, and Y. Cheng, "High-precision propagation-loss measurement of single-mode optical waveguides on lithium niobate on insulator," Micromachines **10**, 612 (2019).
28. J. X. Zhou, R. H. Gao, J. T. Lin, M. Wang, W. Chu, W. B. Li, D. F. Yin, L. Deng, Z. W. Fang, J. H. Zhang, R. B. Wu, and Y. Cheng, "Electro-optically switchable optical true delay lines of meter-scale lengths fabricated on lithium niobate on insulator using photolithography assisted chemo-mechanical etching," Chin. Phys. Lett. **37**, 084201 (2020).
29. P. Rabiei and W. H. Steier, "Lithium niobate ridge waveguides and modulators fabricated using smart guide," Appl. Phys. Lett. **86**, 161115 (2005).
30. H. Hu, J. Yang, L. Gui, and W. Sohler, "Lithium niobate-on-insulator (LNOI): status and perspectives," Proc. SPIE **8431**, 84311D (2012).
31. R. Takigawa, E. Higurashi, T. Kawanishi, and T. Asano, "Lithium niobate ridged waveguides with smooth vertical sidewalls fabricated by an ultra-precision cutting method," Opt. Express **22**, 27733 (2014).
32. M. F. Volk, S. Suntsov, C. E. Rueter, and D. Kip, "Low loss ridge waveguides in lithium niobate thin films by optical grade diamond blade dicing," Opt. Express **24**, 1386 (2016).
33. T. Ding, Y. Zheng, and X. Chen, "Integration of cascaded electro-optic and nonlinear processes on a lithium niobate on insulator chip," Opt. Lett. **44**, 1524 (2019).
34. M. Wang, R. Wu, J. Lin, J. Zhang, Z. Fang, Z. Chai, and Y. Cheng, "Chemo-mechanical polish lithography: a pathway to lowloss large-scale photonic integration on lithium niobateon insulator," Quantum Eng. **1**, e9 (2019).
35. J. Zhang, Z. Fang, J. Lin, J. Zhou, M. Wang, R. Wu, R. Gao, and Y. Cheng, "Fabrication of crystalline microresonators of high quality factors with a controllable wedge angle on lithium niobate on insulator," Nanomaterials **9**, 1218 (2019).
36. V. S. Ilchenko, A. A. Savchenkov, A. B. Matsko, and L. Maleki, "Nonlinear optics and crystalline whispering gallery mode cavities," Phys. Rev. Lett. **92**, 043903 (2004).
37. P. Rabiei and P. Gunter, "Optical and electro-optical properties of submicrometer lithium niobate slab waveguides prepared by crystal ion slicing and wafer bonding," Appl. Phys. Lett. **85**, 4603 (2004).
38. R. Gao, H. Zhang, F. Bo, W. Fang, Z. Hao, N. Yao, J. Lin, J. Guan, L. Deng, M. Wang, L. Qiao, and Y. Cheng, "Broadband highly efficient nonlinear optical processes in on-chip integrated lithium niobate microdisk resonators of *Q* factor above 10^8," arXiv: 2102.00399 (2021).

39. R. Wu, J. Zhang, N. Yao, W. Fang, L. L. Qiao, Z. Chai, J. Lin, and Y. Cheng, "Lithium niobate micro-disk resonators of quality factors above 10^7," Opt. Lett. **43**, 4116 (2018).
40. H. Lee, T. Chen, J. Li, K. Y. Yang, S. Jeon, O. Painter, and K. J. Vahala, "Chemically etched ultra high-*Q* wedge-resonator on a silicon chip," Nat. Photon. **6**, 369 (2012).
41. J. Zhang, R. Wu, M. Wang, Z. Fang, J. Lin, J. Zhou, R. Gao, W. Chu, and Y. Cheng, "High-index-contrast single-mode optical waveguides fabricated on lithium niobate by photolithography assisted chemo-mechanical etching (PLACE)," Jpn. J. Appl. Phys. **59**, 086503 (2020).
42. M. Oxborrow, "Traceable 2-D finite-element simulation of the whispering-gallery modes of axisymmetric electromagnetic resonators," IEEE Trans. Microwave Theory Tech. **55**, 1209 (2007).
43. J. Lin, Y. Xu, J. Ni, M. Wang, Z. Fang, L. Qiao, W. Fang, and Y. Cheng, "Phase-matched second harmonic generation in an on-chip $LiNbO_3$ microresonator," Phys. Rev. Appl. **6**, 014002 (2016).
44. D. E. Zelmon, D. L. Small, and D. Jundt, "Infrared corrected Sellmeier coefficients for congruently grown lithium niobate and 5 mol.% magnesium oxide-doped lithium niobate," J. Opt. Soc. Am. B **14**, 3319 (1997).
45. J. Zhang, R. Wu, M. Wang, Y. Liang, J. Zhou, M. Wu, Z. Fang, W. Chu, and Y. Cheng, "An ultra-high-*Q* lithium niobate microresonator integrated with a silicon nitride waveguide in the vertical configuration for evanescent light coupling," Micromachines **12**, 235 (2021).
46. K. Y. Yang, D. Y. Oh, S. H. Lee, Q.-F. Yang, X. Yi, B. Shen, H. Wang, and K. Vahala, "Bridging ultrahigh-*Q* devices and photonic circuits," Nat. Photon. **12**, 297 (2018).